ELSEVIER

Gas barrier properties of butyl rubber/vermiculite nanocomposite coatings

S. Takahashi [a], H.A. Goldberg [b], C.A. Feeney [b], D.P. Karim [b], M. Farrell [b],
K. O'Leary [a], D.R. Paul [a,*]

[a] Department of Chemical Engineering and Texas Materials Institute, The University of Texas at Austin, Austin, TX 78712, USA
[b] InMat Inc., Hillsborough, NJ 08844, USA

Abstract

Gas barrier properties of butyl rubber/vermiculite nanocomposites coatings are described here. The coating formulations consisting of a butyl rubber latex (the rubber particles are about 1 μm in diameter) to which exfoliated vermiculite was added were applied to a poly(2,6-dimethyl-1,4-phenylene oxide) (PPO) coated Anapore ceramic disc; composites containing 0, 20 and 30 wt% of vermiculite were evaluated. The permeability of the nanocomposite coatings to various gases was measured and compared to permeation models for composites with flake-like fillers proposed by Cussler, Nielsen, Fredrickson and Bicerano, and Gusev and Lusti. The gas permeability of the nanocomposite materials was decreased remarkably by the presence of the high loadings of vermiculite. Diffusion coefficients computed from time lag data also decreased remarkably with the vermiculite content. TEM and SEM were used to observe the internal structure of the nanocomposite membranes in an effort to gain further understanding of the permeability properties. Aspect ratios ranging from 100 to 480 were predicted from the gas permeation results and the above models. TEM experiments could not provide a precise estimate of the aspect ratio but the range predicted from the models are of this order. Apparent solubility coefficients, computed by dividing the experimental permeability by the diffusivity obtained from the time lag observation, increased significantly with vermiculite content in contradiction to the theoretical prediction. Independent gas sorption isotherm experiments for CO_2 were measured and found to be larger than that in butyl rubber possibly due to adsorption on the vermiculite. While this turned out to be a very complicated system, it seems clear from these results that the transient tortuosity factor defined by the time lag is significantly larger than the steady-state tortuosity factor defined by permeability.
© 2006 Elsevier Ltd. All rights reserved.

Keywords: Gas permeation properties; Nanocomposite coatings; Permeation models

1. Introduction

Use of nano-sized filler particles to form polymer composites has attracted much attention in recent years because of the potential performance advantages that could create new technological opportunities. Several review papers on polymer nanocomposites formed from layered silicates have appeared [1–3]. The key issue is to obtain an effective dispersion and exfoliation of the platelets into the polymer matrix to yield well-aligned, high-aspect ratio particles for mechanical reinforcement or a tortuous diffusion pathway for improved barrier properties. Indeed, the literature contains numerous reports on increased modulus and dimensional stability [1–11], increased strength and heat resistance

[1–3,5–7], and decreased gas permeability [1–3,12–23] caused by addition of layered silicates to various polymer matrices. Much of the literature is devoted to nanocomposites made by addition of organoclays, formed from montmorillonite, to thermoplastics using melt-processing techniques. While it is clear that the property benefits of adding plate-like fillers to polymers will increase as both the volume fraction, ϕ, and the aspect ratio, α, of the platelets increase, there are natural limits on both ϕ and α inherent to this approach imposed by the effect such particles have on melt rheology [1,2,23–25].

Goldberg, Feeney and co-workers have recently described a water-based approach for forming elastomeric nanocomposite coatings with high loadings of high-aspect ratio platelets specifically designed for gas barrier applications [26–28]. The purpose of this paper is to explore the permeation characteristics of a series of gases in these materials using experimental techniques developed at the University of Texas at Austin that are readily adaptable for such coatings [29,30]. These coatings are based on butyl rubber, which is well known among elastomers for its superior gas barrier characteristics. The filler

is vermiculite, which is a layered silicate that can be dispersed in water like montmorillonite but its platelets are believed to have a much higher aspect ratio [9,26,31]. The butyl rubber is formed into a latex that is mixed with an aqueous dispersion of vermiculite in the desired ratio. This water-based formation can then be sprayed onto a substrate where the water eventually evaporates to form a continuous coating. High concentrations of the vermiculite platelets should force them into good alignment, which is essential for good barrier performance. The observed gas permeation characteristics are compared with predictions by various theories available in the literature [13,14,20,21].

2. Experimental procedures

The specimen configuration used for gas permeation measurement in this study is composed of three layers as shown in Fig. 1. The support layer is a ceramic Anapore Membrane Disk with 0.02 μm surface pores, manufactured by Whatman International Ltd. The pores of the ceramic support were sealed to prevent subsequent polymer ingression into the pores by coating its surface with 1.5 cm^3 of a poly(2,6-dimethyl-1,4-phenylene oxide) or PPO solution (15 wt% of solids in trichloroethylene) with a syringe. The disk was immediately scraped with a razor blade that removed nearly all the PPO solution; however, some of the solution penetrates into the pores of the ceramic disk. The disk remained covered in the hood for 24 h to evaporate most of the solvent and was then placed in a vacuum oven at 100 °C for another 24 h. Finally, it was placed in a 60 °C oven for 2 weeks for aging as discussed in detail elsewhere [29,30]. Although the PPO 'coating' is very thin, it can contribute to the overall permeation resistance of the composite assembly; therefore, the permeation resistance of this layer to each gas was measured before the butyl rubber–vermiculite nanocomposite coating was added by InMat Inc. using techniques described previously [26–28]. The coating
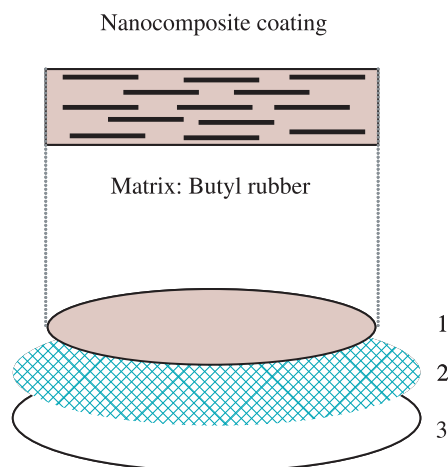
Nanocomposite coating

Fig. 1. Schematic illustration of sample configuration used to make permeation measurements for the butyl rubber based nanocomposites. Layer 1 is the nanocomposite of interest while layer 2 is a thin PPO coating used to prevent the polymer sample from penetrating into the pores (0.02 μm in diameter) of the Anapore ceramic disc (layer 3) used for mechanical support.

technique starts with a butyl rubber latex (the rubber particles are about 1 μm in diameter) to which an aqueous dispersion of exfoliated vermiculite is added. An important and novel feature of these coatings is their mesoscopic structure. This means that locally all the filler particles are aligned because of their high-aspect ratio and the concentration of filler. The technique allows the vermiculite platelets to remain substantially exfoliated and aligned, even in the presence of the butyl rubber and the surfactant used to stabilize the latex, during coating and drying. Formulations containing 0, 20 and 30 wt% of vermiculite were evaluated here; see Table 1. The thickness of these coatings was calculated from the weight of a coated sample by InMat Inc. These coatings contain curatives so they can be vulcanized by heating; however, no curing cycle was employed in this work. The coatings containing vermiculite are analogous to the commercially available products known as Air D-Fense™ 2000 and 3000. The ceramic supports are quite brittle and with the shipping and handling involved breakage was inevitable; however, this was quite apparent when tested for gas permeation. Thus, the data reported here were obtained with samples that showed no evidence of damage to the coating, judged primarily by the observed permselectivity.

Gas permeation through the nanocomposite assemblies was measured at 30 °C for He, H$_2$, O$_2$, N$_2$, CH$_4$ and CO$_2$ at an upstream pressure of about 2 atm using a constant pressure/variable volume type permeation cell used in this laboratory and described in detail elsewhere [32,33]. The data can be represented as the amount of gas that has permeated, Q_t, as a function of time, t. Eventually, the plot of Q_t versus t becomes linear from which a steady-state (ss), pressure normalized flux or permeance, $(P/l)_a$, for the entire assembly can be calculated as follows

$$\left(\frac{P}{l}\right)_a = \frac{(dQ_t/dt)_{ss}}{A\Delta p} \tag{1}$$

where A is the permeation area and Δp is the pressure driving force. The permeance of the nanocomposite coating, P/l, is computed by subtracting out the contribution of the PPO layer, i.e.

$$\left(\frac{l}{P}\right)_{coating} = \left(\frac{l}{P}\right)_a - \left(\frac{l}{P}\right)_{PPO} \tag{2}$$

Typically, this correction was always less than 10%. The permeability of the nanocomposite was then calculated from

Table 1
Nanocomposite samples used in this study

Sample[a]	Vermiculite[b]		Thickness (μm)
	(wt%)	(vol%)	
A	0	0	82.8
B	20	8.4	23.9
C	30	13.6	18.2

[a] The butyl rubber is reported to have $\bar{M}_w = 600,000$. All formulations contained curatives used for crosslinking.
[b] Volume percents were calculated using densities of 0.92 g/cm^3 for the butyl rubber and 2.5 g/cm^3 for vermiculite.

the measured permeance and measured thickness. Extrapolation of the Q_t versus t plot in the steady-state region to the time axis gives the time lag θ. The effective time lag of the PPO layer was too short to be measured.

Thin sections of the nanocomposites for transmission electron microscopy (TEM) ranging from 20 to 30 nm in thickness were cut with a diamond knife at a temperature of $-120\,°C$ using a Power Tome Ultramicrotome Model XL, Boeckeler Instruments, Inc. In this process, the sample was supported by epoxy resin to facilitate cutting. The sections were collected on 300 mesh square copper grids and subsequently dried with filter paper. The sections were examined by TEM using a JEOL 2010F TEM at an accelerating voltage of 120 kV. An Hitachi S-4500 field emission scanning electron microscope (SEM) operated at a voltage of 15 kV was used to view cross-sections formed by cleaving the nanocomposite using tweezers while in the presence of liquid nitrogen that were subsequently coated with gold.

Solubility measurements were carried out using a pressure decay method as a function of temperature in a dual volume described previously [34]. Measurements were made using CO_2 because it has a high solubility in butyl rubber; the other gasses have much lower solubility levels that greatly compromises the accuracy of measurement. The effect of non-ideal gas behavior was accounted for by using compressibility factors [35]. The coating sample used in this measurement were prepared separately and applied via spray coating on aluminum foil that was taken off prior to use.

3. Review of composite theories for permeation

The simple solution–diffusion description of the steady-state transport of a penetrant in a homogeneous polymer matrix indicates that the permeability coefficient, P, is the product of solubility, S, and diffusivity, D, coefficients, i.e.

$$P = DS \tag{3}$$

A similar form has been assumed to apply for composites comprised of particles, which do not sorb or conduct the penetrant, dispersed in a matrix whose local characteristics are assumed to be unaffected by the presence of the particles. The latter assertion is an assumption of 'composite theory' and its validity should be tested when the particles are very small or have a high surface to volume ratio as is the case for so-called 'nanocomposites'.

Simple composite theory for the type of systems mentioned above, in the absence of adsorption by the filler or effects of the filler on the surrounding polymer matrix, would predict the penetrant solubility in the composite to be

$$S = S_0(1-\phi) \tag{4}$$

where S_0 is the penetrant solubility coefficient in the pure polymer matrix and ϕ is the volume fraction of particles dispersed in the matrix. In this approximation, the solubility does not depend on the morphological features of the phases.

However, the diffusion process is more complex. The particles act as impenetrable barriers so that the penetrant must follow an elongated, or tortuous, path in order to diffuse through the composite. This can be accounted for by a tortuosity factor, f:

$$D = D_0 f \tag{5}$$

According to simple composite theory, this tortuosity factor depends on the content of particles, ϕ; the particle shape, e.g. an aspect ratio, α; and the location and orientation of the particles in space; however, it should not depend on absolute particle size or what the penetrant is. Combining the above equations gives

$$P = DS = (1-\phi)S_0 D_0 f = (1-\phi)P_0 f \tag{6}$$

or
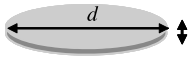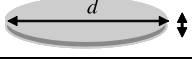
$$f \equiv \frac{P}{P_0(1-\phi)} \tag{7}$$

where P_0 is the penetrant permeability coefficient in the pure polymer matrix. In principle, this impedance or tortuosity factor, f, can be calculated by an appropriate solution to Fick's law if a complete description of the two-phase morphology is known. There is an extensive literature devoted to this problem using varying approaches and levels of sophistication or approximation [13–21,36].

We will focus here only on those theories dealing with particles having a plate-like shape [13–21]; these theories are summarized in Table 2 by giving the reciprocal of the predicted tortuosity factor f^{-1}. These theories fall into two categories. The first deals with what will be called 'ribbons' here. These are rectangular platelets with finite width, w, and thickness, t, but infinite in length. We characterize their aspect ratio as $\alpha = w/t$. Nielsen assumed a specific regular array of ribbons and calculated f^{-1} from simple geometrical considerations. Cussler et al. [14] formulated the consideration of regular and random arrays of ribbons somewhat differently and obtained the results included in Table 2. The papers from this group include various versions of the predicted results. Some are inconsistent in that they equate the reductions in permeability and diffusivity such that the factor $(1-\phi)$ appears in some versions but not others. We have taken the liberty of writing their equations as outlined above. Attempts to account for other orientations have been reported [19].

The second category of plate-like theories employs circular disks of diameter, d, and thickness, t. We characterize their aspect ratio as $\alpha = d/t$. These theories allow for random placement of disks in space but assume they are oriented within the plane of the film or membrane [20,21]. Gusev and Lusti [20] performed a series of finite-element analyzes of a random dispersion of non-overlapping impermeable round platelets for a number of values of α and ϕ. They found that the results in the form of P_0/P could be represented by the stretched exponential function shown in Table 2. Note that we have taken the liberty of adding the factor $(1-\phi)$ for the reason outlined above; Gusev and Lusti did not include this factor in their correlation. Fredrickson and Bicerano [21] approached the analogous diffusion problem using a second-order

Table 2
Detailed schematics and formulas for each model discussed in the text

Model	Filler type	Particle geometry	Formulas	References
Nielsen	Ribbon[a]	*w*, *t*	$(P_0/P)(1-\phi) = 1 + \alpha\phi/2$	[13]
Cussler (Regular array)	Ribbon[a]	*w*, *t*	$(P_0/P)(1-\phi) = 1 + (\alpha\phi)^2/4$	[14]
(Random array)			$(P_0/P)(1-\phi) = (1 + \alpha\phi/3)^2$	[14]
Gusev and Lusti	Disk[b]	*d*, *t*	$(P_0/P)(1-\phi) = \exp[(\alpha\phi/3.47)^{0.71}]$	[20]
Fredrickson and Bicerano	Disk[b]	*d*, *t*	$(P_0/P)(1-\phi) = 4((1 + x + 0.1245x^2)/(2 + x))^2$ where $x = \pi\alpha\phi/2 \ln(\alpha/2)$	[21]

[a] For ribbons, length is infinite, width, *w*; thickness, *t*; aspect ratio, $\alpha \equiv w/t$.
[b] For disks, circular shape of diameter *d* and thickness *t*; aspect ratio, $\alpha \equiv d/t$.

approximation from a multiple scattering formulation to obtain the expression in Table 2. It is important to note that Table 2 uses a consistent set of definitions for the particle aspect ratios which in some cases is not the definition used in the original papers. Thus, the equations given here differ from the original papers in this way and by consistently incorporating the $(1-\phi)$ factor required by Eq. (4).

The transient permeation experiment also gives the diffusion time lag θ, which for a simple homogeneous film of thickness l_0 is given by
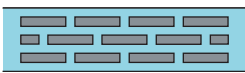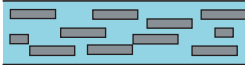
$$\theta_0 = \frac{l_0^2}{6D_0} \tag{8}$$

If we assume that the simple composite formalism given above applies, then we may compare the time lag for a composite to that of the neat polymer as follows

$$\frac{D_0}{D} = \left(\frac{l_0}{l}\right)^2 \left(\frac{\theta}{\theta_0}\right) = f^{-1} \tag{9}$$

where allowance is made for the fact that the two films being compared may not have the same thickness; this is clearly the case in the current experiments, see Table 1. Cussler et al. have given equivalent expressions for θ, based on slightly different arguments, for their prediction models, see Table 3. Eq. (9) suggests that the same expression, f, that predicts P should also predict θ; however, numerous papers have suggested the tortuosity factor in a transient experiment, f_{tr}, may not be the same as in a steady-state experiment, f_{ss}, i.e. $f_{tr} \neq f_{ss}$ [37–40].

4. Results and discussion

4.1. Electron microscopy observations

Fig. 2 shows SEM micrographs of edge views of cryofractured butyl rubber membranes containing 20 and 30 wt% of vermiculite. Owing to the irregular nature of the fracture surface and the relatively low magnification, it is difficult to say much about the local morphology of the composites. However, it is quite apparent that the vermiculite layers are well aligned within the plane of the membrane as expected based on the method of preparation outlined earlier.

Figs. 3 and 4 show representative TEM micrographs taken of microtomed cross-sections from butyl rubber membranes containing 20 and 30 wt% of vermiculite. These represent but a few of many attempts to image the morphology of these composites. It is important to understand that it is very difficult to cleanly cut sections of these materials because of the very low-glass transition temperature, about −80 °C, of the butyl rubber matrix. The thin sections were invariably wrinkled and otherwise distorted. These difficulties stem from ensuring that the butyl rubber matrix is indeed below its T_g, and therefore rigid, at the surface being cut plus the distortions that arise from warming to room temperature which relieves stresses induced by cutting. Given these limitations, it appears that these composites consist of a mixture of individual vermiculite platelets and some stacks of platelets. The well-dispersed platelets appear to be 1–2 nm in thickness and 200–400 nm in length. The thicker stacks are several microns in length. The wavy or curved type structures seen in Fig. 4 have been observed in other nanocomposites formed from layered silicates made

Table 3
Cussler models for the time lag. Ref. [14]

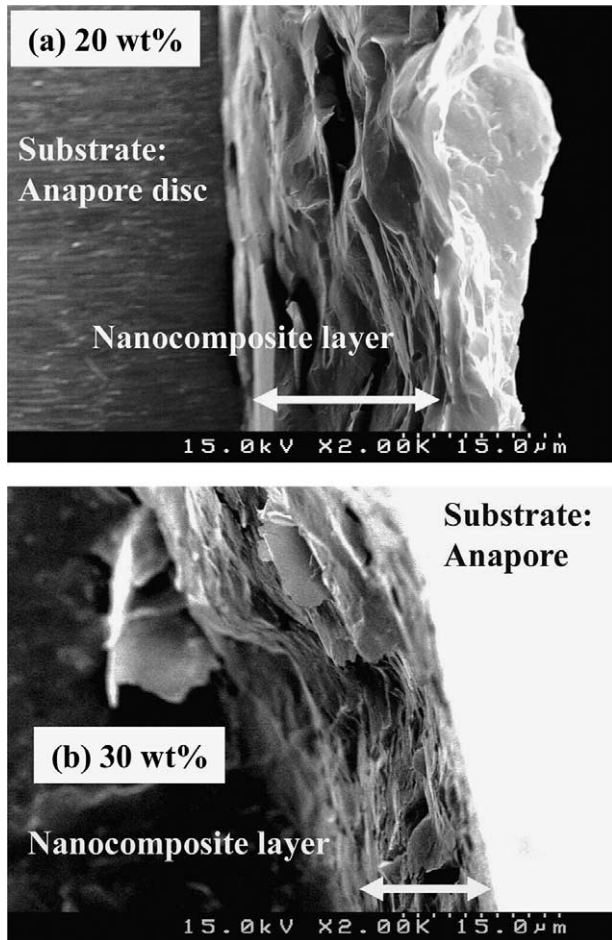| Model	Filler type	Model geometries	Formula
Cussler (Regular array)	Ribbon		$(\theta/\theta_0) = 1 + ((\alpha\phi)^2/4)$
(Random array)			$(\theta/\theta_0) = (1 + (\alpha\phi/3))^2$

Fig. 2. SEM views of cross-sections obtained by cryofracturing of the nanocomposite test assembly (a) sample B containing 20 wt% vermiculite and (b) sample C containing 30 wt% vermiculite.

quantification of this important morphological feature seems essentially impossible because of the difficulties mentioned already and the further complications of defining the lateral dimensions of large particle within the limited field of view dictated by the high magnification needed to observe the particles. From these and other TEM micrographs, one can easily believe that the aspect ratio might be in the range of 100–400; however, we cannot be more specific.

4.2. Steady-state gas permeation properties

As previously noted, the gas permeability coefficients of the nanocomposite membranes were calculated from data like that in Fig. 5 using Eqs. (1) and (2). The measured gas permeability coefficients for butyl rubber with and without vermiculite are listed in Table 4; our butyl rubber data are in substantial agreement with the data from the literature [42]. The slight deviations seen in Table 4 can be attributed in part to errors in estimating the membrane thickness; however, the uncertainty due to this is less than 10%. Samples B with 20 wt% vermiculite and C with 30 wt% vermiculite showed significantly lower permeability coefficients for all gases than sample A, i.e. butyl rubber without vermiculite.

The data are summarized in Fig. 6 as a plot of relative permeability, P/P_0, versus the mass content of vermiculite in the membrane. For each gas and membrane composition, the relative permeability was computed by dividing the observed permeability coefficient by the experimental permeability coefficient, P_0, of that gas in the membrane containing no vermiculite. According to the general Eqs. (5) and (6) or the specific models in Table 2, the relative permeability for a given butyl rubber/vermiculite membrane should be the same for all gases. However, as seen in Fig. 6, the relative permeability for the various gases may differ by as much as a factor of two for a given membrane. The essential question is whether this variation represents experimental error or a real deviation from the assumptions behind Eqs. (5) and (6). We will return to this question later after examining the broader trends and comparisons with the various models summarized in Table 2.

using very different materials and processes [41]. At the present time, it is not possible to explain the origin of such structures or to know if they are truly representative of the morphology or simply artifacts of the microtoming. It was hoped that these TEM observations would lead to an experimental assessment of the aspect ratio of the vermiculite particles. However,
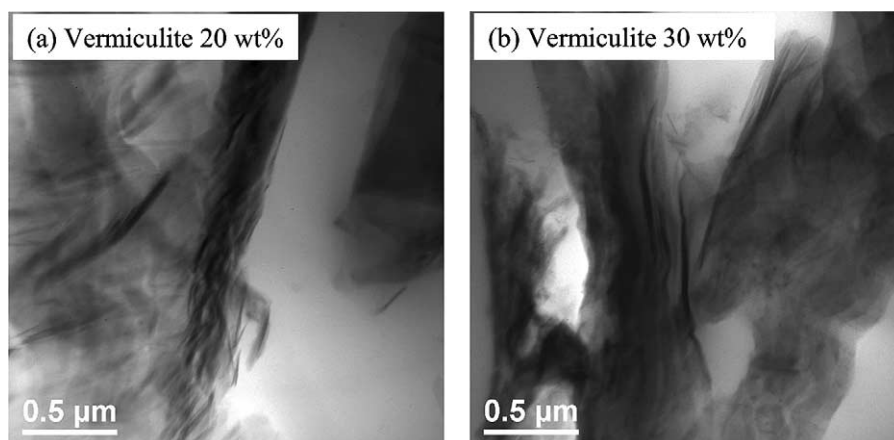

Fig. 3. TEM micrographs of thin cryomicrotomed sections, viewed at 120 kV, of sample B (20 wt% vermiculite), (a), and sample C (30 wt% vermiculite), (b).
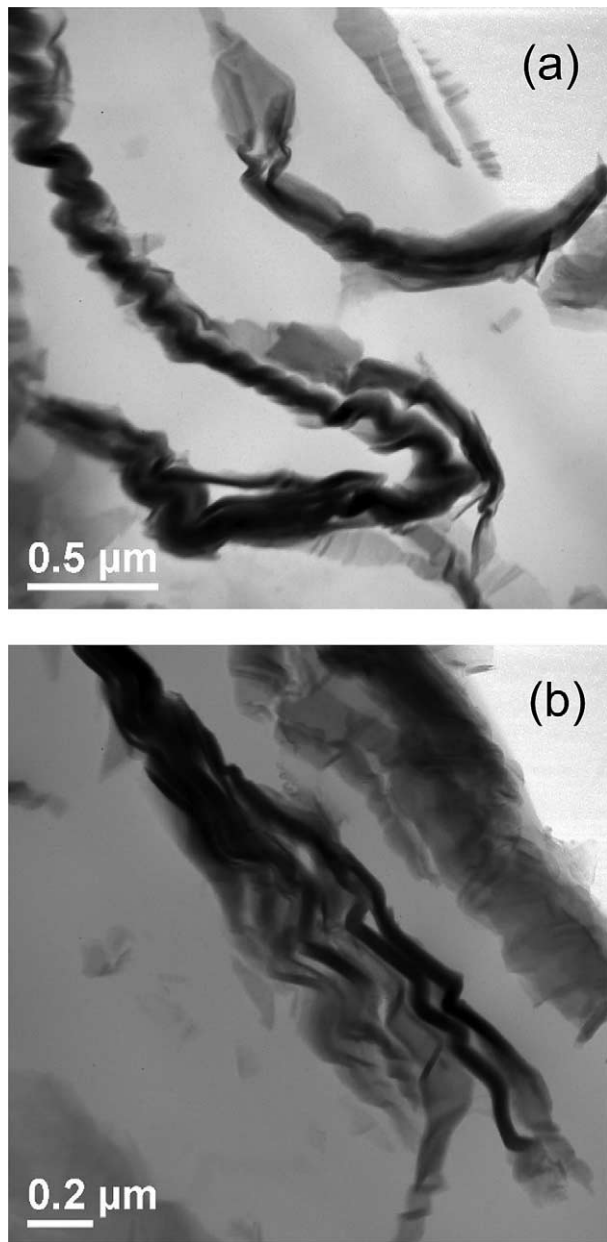
Fig. 4. TEM images of thin sections of sample B (20 wt% vermiculite) revealing curved and twisted platelet stacks.

4.3. Comparison of steady-state permeation data with theoretical models

The composite theories described earlier suggest that the tortuosity factor f that can be computed from experimental permeability data using Eq. (7) should be a function of only ϕ and α. Since the volume fraction of vermiculite can be computed from the composition of the membrane and the densities of components, we could make absolute comparisons of the experimental data with the predictions of the various theories if we knew α. However, as explained earlier, it does not seem feasible to determine the aspect ratio independently using, for example, electron microscopy. Even if we could independently know the distribution of lateral platelet
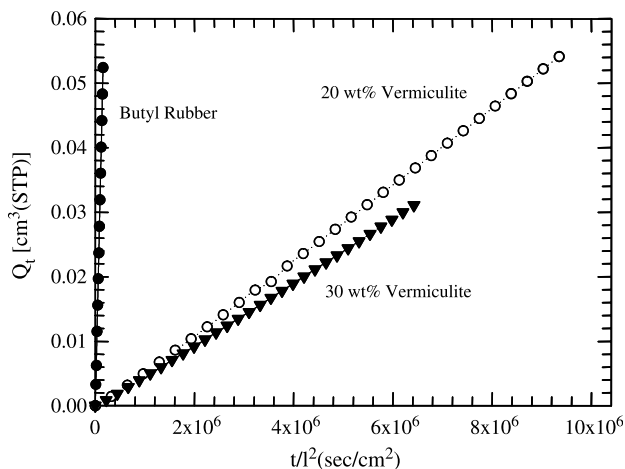

Fig. 5. Comparison of accumulative amount of oxygen that exits the membrane in a transient permeation test as a function of time normalized by thickness for sample with various amounts of vermiculite.

dimensions of the vermiculite material used to form the coatings, there are other key morphological details like spatial distribution and incomplete exfoliation that would be unknown and prohibit a straightforward comparison of the data with the various theories. Consequently, we take a more pragmatic path which if nothing else shows the very large differences in the predictions given by the various theories.

The Nielsen theory expresses f as a function of the product $\alpha\phi$ as seen in Table 2. The Cussler theories as well as that by Gusev and Lusti (GL) are also of this form if we incorporate the logical $(1-\phi)$ term as described earlier. However, the Fredrickson and Bicerano (FB) theory has a functional form that requires α in addition to the product $\alpha\phi$ since it contains the term $x = \pi\alpha\phi/2 \ln(\alpha/2)$. In Fig. 7, we plot the reciprocal quantity, f^{-1}, versus the product $\alpha\phi$ over the expected range. Because of the nature of the FB form, it is necessary to do this at a specified value of ϕ; thus, we have chosen to show the plots corresponding to the volume fractions of the 20 and 30% by weight vermiculite compositions. For the FB case, we did the
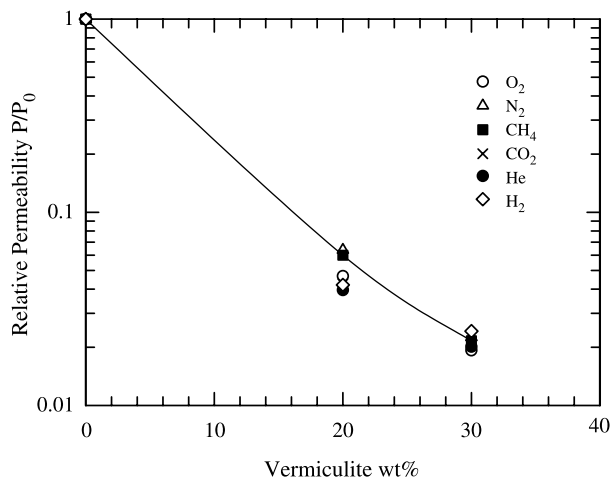

Fig. 6. Relative permeability of various gases in butyl rubber/vermiculite nanocomposites as a function of vermiculite content. Measurements were carried out at 30 °C and 2 atm.

Table 4
Gas permeability coefficients and selectivity for nanocomposite samples used in this study

Sample	Gas permeability coefficients (Barrer)						O_2/N_2	CO_2/CH_4	He/N_2	CO_2/N_2	He/H_2	He/O_2	He/CO_2	O_2/CO_2
	H_2	He	O_2	N_2	CH_4	CO_2								
Literature[a]	7.22	8.41	1.30	0.323	–	5.17	4.02	–	26.02	16.01	1.16	6.47	1.63	3.98
A	6.51	7.63	1.28	0.324	0.751	5.00	3.95	6.67	23.56	15.45	1.17	5.96	1.52	3.91
B	0.257	0.321	0.0599	0.0207	0.0450	0.214	2.90	4.75	15.53	10.33	1.25	5.36	1.50	3.57
C	0.131	0.185	0.0247	0.0073	0.0162	0.106	3.38	6.53	25.37	14.51	1.41	7.50	1.75	4.29

[a] Literature data for butyl rubber from Ref. [42].

calculation by expressing x as $(\pi y/2)/\ln(y/2\phi)$ where y is the combination of variables $\alpha\phi$, i.e. the abscissa in Fig. 7, and ϕ in the filler content with values of 0.0842 or 0.1362. This causes some singularities in f^{-1} at low $\alpha\phi$; however, the functional form of this version is well behaved in the $\alpha\phi$ region of interest.

The various models predict very different results in some cases. The Cussler models predict the greatest tortuosity effect at a given $\alpha\phi$ while the Nielsen and FB models predict the least effect. The latter two predictions are quite similar as noted earlier [21]. The GL model predicts results in between these extremes. Clearly, it would be of interest to know which theory provides the best absolute approximation to real composites; however, since we cannot independently determine α with any certainty, we will not be able to resolve that question here. Interestingly, the Cussler and Nielsen models are based on ribbons and not disks. The fact that these two theories represent the two extremes clearly indicates that this geometrical simplification compared to disks is not the major issue behind the wide variation in predictions.

On each of the two plots in Fig. 7, we have drawn horizontal lines corresponding to the experimentally determined value f^{-1} for each gas in each composite membrane. From the known ϕ, we can determine what α each theory would require in order to predict that f^{-1}. In Table 5, we show the range of α needed to describe the results for the various gases in each membrane. If we ignore for a moment the details of any specific effects associated with a given gas or value of ϕ, we can reduce the range to an average α as given in the last line in Table 5. These α range from 100 to 480. We have inserted these values into the respective theory and compare the predicted reduced permeability versus ϕ with the experimental results in Fig. 8. If one treats α as an adjustable parameter within the various models, we see that their predictions are rather similar and within the range of experimental variation among the gases. Thus, this is not a viable way to determine which is the better model.

4.4. Transient permeation results and analysis

A simple interpretation of Eqs. (8) and (9) imply that the effective diffusion coefficient for any gas in a composite membrane, as defined by Eq. (5), can be computed from the observed time lags (Fig. 5). Fig. 9 shows the diffusion coefficients computed in this way normalized by the similarly computed diffusion coefficient for that gas in butyl rubber without vermiculite, i.e. D_0 determined from sample A in Table 1. No results are included for helium and hydrogen since their time lags were too short to be measured accurately, particularly for sample A. Again, the general composite theory outlined earlier implies that for each nanocomposite, that the relative diffusion coefficient should be the same for all gases. As with the relative permeability, there is a spread in the values obtained for different gases of the order of a factor of two. We see that the diffusion coefficients determined in this way are reduced by two orders of magnitude (Fig. 9) at the highest loadings of vermiculite, whereas, the steady-state permeability coefficients are reduced by factors of 25–30 (Fig. 6).
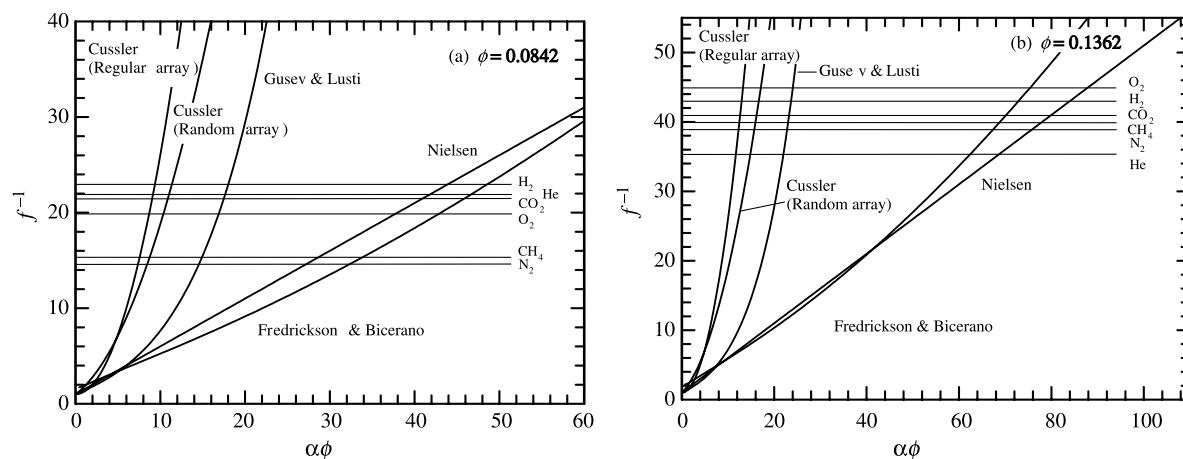
Fig. 7. The reciprocal tortuosity factor predicted by the various theories as a function of $\alpha\phi$. Horizontal lines correspond to experimental values for each gas computed from permeability. Part (a) is for a vermiculite content of $\phi=0.0842$; part (b) is for a vermiculite content of $\phi=0.1362$.

As suggested by Eq. (3), the solubility coefficient for each gas and membrane composition can be calculated by dividing the experimental permeability by the diffusivity obtained from the time lag observation using Eq. (8). As suggested by Eq. (4), the solubility coefficient should decrease with filler loading since the volume of available polymer is decreased. However, as seen in Fig. 10, the relative solubility coefficients computed as described increase significantly with vermiculite content in contradiction to the theoretical prediction of Eq. (4). To better understand this, independent gas sorption experiments were made for CO_2 in samples A and C with the results shown in Fig. 11. Most likely some gas is adsorbed at the vermiculite surface. Both experimental sorption isotherms are linear, i.e. Henry's law applies; however, the slope of the CO_2 isotherm for the sample containing 30% by weight vermiculite is higher than that containing no vermiculite by a factor of 1.37. However, the equilibrium sorption isotherm does not yield solubility coefficients as high as the values computed from the steady-state permeability and time lag, see Fig. 10. It appears that multiple issues may contribute to these discrepancies.

First, it appears that vermiculite filler or the filler–polymer interfacial region contribute to the extra sorption observed in the composite as shown by the equilibrium CO_2 sorption results shown in Fig. 11. If the CO_2 molecules held in this excess sorption mode are immobilized, then this will tend to lengthen the time lag from that expected by the increased tortuous path the gas molecules must follow to pass through the filled polymer.

A further effect may be that the tortuosity factor for steady-state diffusion in filled polymer as defined by Eq. (5) may not

be applicable for a transient permeation experiment. Indeed, several earlier authors have advocated this and have shown experimental results that are consistent with the idea [37,38]. Thus, to account for this in a formal way we write for steady-state permeation

$$D = D_0 f_{ss} \tag{10}$$

to define the steady-state tortuosity factor f_{ss}. For the transient permeation experiment in a filled system, without any effects of immobilizing adsorption by the filler, we write

$$\theta = \frac{l^2}{6D_{tr}} \tag{11}$$

where we define the transient tortuosity factor f_{tr} as

$$D_{tr} = D_0 f_{tr} \tag{12}$$

where, in general, $f_{tr} \neq f_{ss}$. One physical reason for the latter would be that fillers of complex shapes, like incompletely dispersed layered minerals such as vermiculite or montmorillonite, can have passageways that penetrant molecules may enter but not find an escape except back through the entry. This is the 'dead-end' pore idea that has been extensively discussed in the literature [39,40]. Such dead-end pores may lead to $f_{tr} < f_{ss}$.

Yet another possible effect is that the presence of the particle may indeed change the nature of the polymer in close proximity to it by changes in polymer segmental packing and the effect of the force field imposed by the solid particle. Such effects are expected to be exaggerated when the particles are very small, at least in one-dimension and, thus, have high-surface area. A great deal has been

Table 5
Aspect ratio calculated by comparison of experimental permeation data with the various composite theories

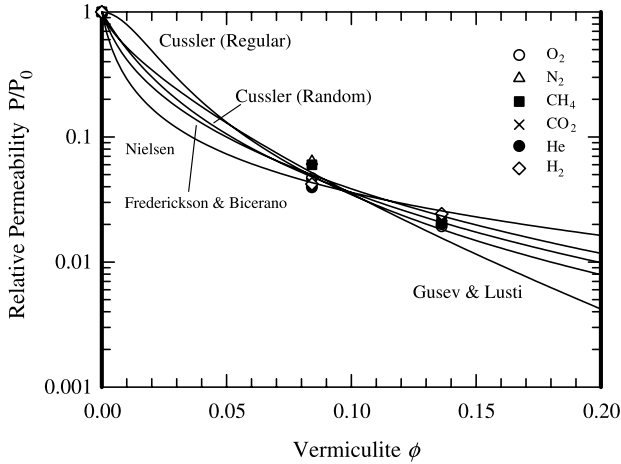| ϕ	Aspect ratio α				
	Nielsen	Cussler (regular)	Cussler (random)	Fredrickson and Bicerano	Gusev and Lusti
0.0842	317–527	87–112	100–137	367–587	171–225
0.1362	508–644	88–97	109–125	461–553	162–176
Average	480	100	120	475	190

Fig. 8. Comparison of experimental data and model predictions of relative permeability calculated from the various theories using the α value that best matches the experimental data (Table 5).

Fig. 10. Relative solubility for various gases in butyl rubber/vermiculite nanocomposites as a function of vermiculite content. The points for N_2 and CO_2 at $\phi = 0.0842$ were shifted slightly to be visible.

written about the possibility of such effects, but no general formulation has been offered for quantitatively interpreting permeation behavior in these terms. At this preliminary stage of development, it seems expedient in the current case to allow any such effects to be incorporated into the tortuosity factor defined above.

To quantify the adsorption effect so that it can be separated from the tortuosity issues, we write the linear equilibrium sorption isotherm describing the results for the composite shown in Fig. 11 as follows

$$C = S_0(1-\phi)p + S_{ex}p \tag{13}$$

or the following equilibrium solubility coefficient

$$S_{eq} = S_0(1-\phi) + S_{ex} \tag{14}$$

The lead term is the expected result, in the absence of adsorption by the filler, as given in Eq. (4) [43–45]. The excess
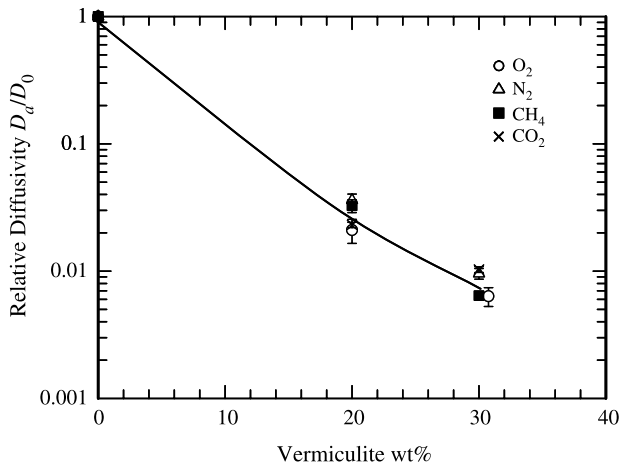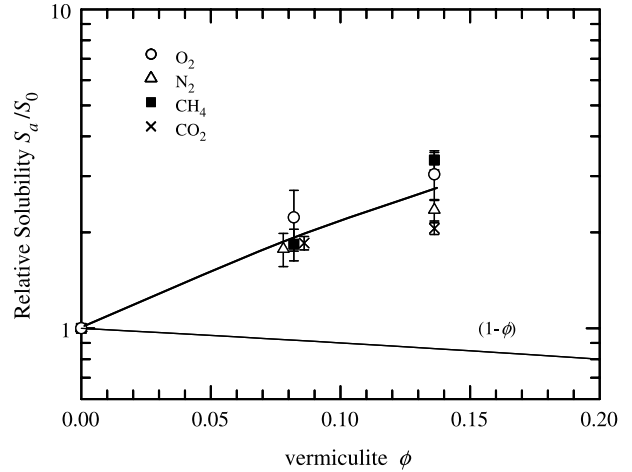
term, S_{ex}, accounts for the adsorption observed regardless of its mechanistic origin. Paul and Kemp [46,47] developed a theory for the time lag in systems with immobilizing adsorption and validated the results by model experiments. In the limit of a linear isotherm, this theory predicts the following time lag relationship

$$\frac{6\theta D_{tr}}{l^2} = 1 + K \tag{15}$$

where in the linear limit we can relate K to the terms in Eq. (14) by

$$K = \frac{S_{ex}}{S_0(1-\phi)} \tag{16}$$

and

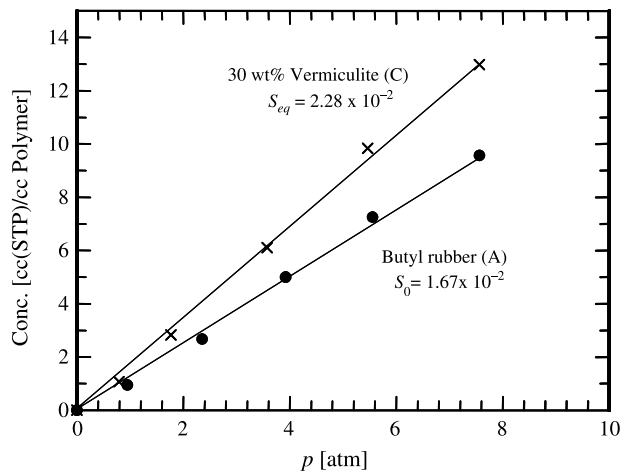$$1 + K = \frac{1}{(1-\phi)}\left(\frac{S_{eq}}{S_0}\right) \tag{17}$$

Fig. 9. Relative diffusivity for various gases in butyl rubber/vermiculite nanocomposites as a function of vermiculite content. The O_2 data point at 30 wt% vermiculite was shifted slightly to the right to be visible.

Fig. 11. Representative CO_2 sorption isotherms for sample A (butyl rubber) and C (30 wt% vermiculite composite) at 30 °C. Units for the solubility coefficients = cm^3 (STP)/cm^3 polymer/cm Hg.

The apparent solubility coefficients, S_a, shown in Fig. 10 were computed from the simple relationship $P = D_a S_a$ where

$$D_a = \frac{D_{tr}}{1 + K} = \frac{D_0 f_{tr}}{1 + K} \tag{18}$$

It is these apparent diffusion coefficients, D_a, that are plotted in Fig. 9. Combining the above equations, we get

$$S_a = \frac{P}{D_a} = \frac{(1 - \phi)S_0 D_0 f_{ss}}{D_0 f_{tr}} \left[\frac{S_{eq}}{S_0(1 - \phi)} \right] \tag{19}$$

or

$$\frac{S_a}{S_0} = \left(\frac{S_{eq}}{S_0} \right) \frac{f_{ss}}{f_{tr}} \tag{20}$$

For carbon dioxide, $S_a/S_0 = 2.06$ and $S_{eq}/S_0 = 1.37$; thus, we calculate $f_{ss}/f_t = 1.46$. This represents a significant difference between the steady state and transient tortuosity factor. It would be interesting to apply similar analysis to the other gases; however, the currently available sorption measurement capabilities do not permit obtaining the needed data with adequate accuracy. The entire question of how different f_{ss} and f_{tr} might be deserves a more intensive investigation but is beyond the current scope of work.

4.5. Effect of gas molecule type

According to the general Eqs. (5) and (6), the relative permeability for a given butyl rubber/vermiculite membrane should be the same for all gases. However, as seen in Fig. 6, the variation in relative permeability among the gases studied may vary by nearly two-fold. The relative diffusivity and solubility computed from transient permeation experiments have a comparable variation (Figs. 9 and 10).

The relative coefficients mentioned involves, of course, a ratio so consequently errors in both the numerator and the denominator are compounded. Clearly, the time lag results are the most prone to experimental error, so it does not seem worthwhile belaboring any trends among different gases molecules for the relative diffusion or solubility coefficients shown in Figs. 9 and 10. For permeability, it is instructive to look at the selectivity, or the ratio of the permeability of various gas pairs, as shown in Table 4. After examining these values carefully, the only clear trend that becomes evident is the selectivity for sample B (20 wt% vermiculite) is essentially always lower than that for the sample with no vermiculite (sample A) or the one containing 30% vermiculite (sample C). There is no obvious explanation for this; however, defects in these assemblies are a significant possibility and this suggests that it would not be fruitful to pursue molecular mechanistic interpretations any further.

The absence of independent sorption data of the type shown in Fig. 11 for other gases and compositions further compromises our ability to give further interpretations. However, generating this data was beyond the scope of what was possible here.

5. Conclusions

Gas permeation properties of nanocomposites based on butyl rubber with high loadings of vermiculite, viz. 20 and 30 wt%, were investigated in this study. The gas permeability is reduced by 20–30-fold by the vermiculite. Diffusion coefficients computed from time lag data were reduced by two orders of magnitude. The experimental data were compared with various models for composites containing flake-like fillers. The range of particle aspect ratios required to make the various models match the experimental data was found to be from 100 to 480. These results are within the range observed by TEM experiments; however, it was not possible to obtain a precise and independent determination of particle aspect ratio by microscopy. Thus, it was not possible to decide which of the various theories provides the best prediction. Solubility coefficients were computed by dividing the experimental permeability by the diffusivity obtained from the time lag observation; these values increased significantly with vermiculite content in contradiction to that expected by theory. Thus, independent gas sorption isotherm experiments were made for CO_2 on butyl rubber compositions with 0 and 30 wt% vermiculite. These results also showed larger solubility in the nanocomposite than in the neat butyl rubber but the extent was not as great as the values discussed above. The excess sorption appears to be the result of gas adsorption by the vermiculite. We rationalize the various observations by considering that the transient tortuosity factor f_{tr} is different from the steady-state tortuosity factor f_{ss} as suggested in the prior literature. For fillers of complex shapes, like incompletely dispersed layered silicates, there are passageways that penetrant molecules may enter but not find an escape except back through the entry, so-called 'dead-end' pores. Such dead-end pores may lead to $f_{tr} < f_{ss}$.

References

[1] Sinha Ray S, Okamoto M. Prog Polym Sci 2003;28:1539–641.
[2] Giannelis EP. Appl Organomet Chem 1998;12:675–80.
[3] Giannelis EP. Adv Mater 1996;8:29–35.
[4] Usuki A, Koiwai A, Kojima Y, Kawasumi M, Okada A, Kurauchi T, et al. J Appl Polym Sci 1995;55:119–23.
[5] Dennis HR, Hunter DL, Chang D, Kim S, Ehite JL, Cho JW, et al. Polymer 2001;42:9513–22.
[6] Kojima Y, Usuki A, Kawasumi M, Okada A, Fukushima Y, Kurauchi T, et al. J Mater Res 1993;8:1185–9.
[7] Sur GS, Sun HL, Lyu SG, Mark JE. Polymer 2001;42:9783–9.
[8] Liu L, Qi Z, Zhu X. J Appl Polym Sci 1999;71:1133–8.
[9] Du X, Xiao M, Meng Y, Hay AS. Polym Int 2004;53:789–93.
[10] Tjong SC, Meng YZ, Xu Y. J Appl Polym Sci 2002;86:2330–7.
[11] Tjong SC, Meng YZ. J Polym Sci, Part B: Polym Phys 2003;41:1476–84.
[12] Yano K, Usuki A, Okada A. J Polym Sci, Part A: Polym Chem 1997;35:2289–94.

[13] Nielsen LE. J Macromol Sci (Chem) 1967;A1:929–42.

[14] Lape NK, Nuxoll EE, Cussler EL. J Membr Sci 2004;236:29–37.

[15] Perry D, Ward WJ, Cussler EL. J Membr Sci 1989;44:305–11.

[16] Lape NK, Yang C, Cussler EL. J Membr Sci 2002;209:271–82.

[17] Yang C, Smyrl WH, Cussler EL. J Membr Sci 2004;231:1–12.

[18] Falla WR, Mulski M, Cussler EL. J Membr Sci 1996;119:129–38.

[19] Bharadwaj RK. Macromolecules 2001;34:9189–92.

[20] Gusev AA, Lusti HR. Adv Mater 2001;13:1641–3.

[21] Fredrickson GH, Bicerano J. J Chem Phys 1999;110:2181–8.

[22] Sinha Ray S, Yamada K, Okamoto M, Ogami A, Ueda K. Chem Mater 2003;15:1456–65.

[23] Sinha Ray S, Okamoto K, Okamoto M. Macromolecules 2003;36: 2355–67.

[24] Fornes TD, Yoon PJ, Hunter DL, Keskkula H, Paul DR. Polymer 2002;43: 5915–33.

[25] Krishnamoorti R, Giannelis EP. Macromolecules 1997;30:4097–102.

[26] Goldberg HA, Feeney CA, Karim DP, Farrell M. Rubber World 2002; 226:15–17 see also p. 20 and 37.

[27] Feeney CA, Farrell M, Tannert K, Goldberg HA, Lu M, Grah MD, et al. United States Patent No. 6,087,016. Assigned to InMat LLC and Michelin Recherche et technique SA; 2000.

[28] Feeney CA, Farrell M, Tannert K, Goldberg HA, Lu M, Grah MD, et al. United States Patent No. 6,232,389. Assigned to InMat LLC and Michelin Recherche et technique SA; 2001.

[29] Mogri Z, Paul DR. Polymer 2001;42:2531–42.

[30] O'Leary K, Paul DR. Polymer 2004;45:6575–85.

[31] Xu J, Meng YZ, Li RKY, Xu Y, Rajulu AV. J Polym Sci, Part B: Polym Phys 2003;41:749–55.

[32] O'Brien KC, Koros WJ, Barbari TA, Sanders ES. J Membr Sci 1986;29: 229–38.

[33] Barbari TA, Koros WJ, Paul DR. J Polym Sci, Part B: Polym Phys 1988; 26:709–27.

[34] Koros WJ. PhD Dissertation, The University of Texas at Austin; 1977.

[35] Dymond JH, Smith EB. The virial coefficients of pure gases and mixtures: a critical compilation. New York: Oxford University Press; 1980.

[36] Maxwell JC. Treatise on electricity and magnetism, vol. I. London: Clarendon Press; 1881.

[37] Paul DR. J Polym Sci, Part A-2 1969;7:1811–8.

[38] Paul DR, Koros WJ. J Polym Sci, Polym Phys 1976;14:675–85.

[39] Goodknight RC, Fatt I. J Phys Chem 1961;65:1709–12.

[40] Fatt I. J Phys Chem 1962;66:760–2.

[41] Stretz HA, Paul DR, Li R, Keskkula H, Cassidy PE. Polymer 2005;46: 2621–37.

[42] Brandrup J, Immergut EH, Grulke EA. Polymer handbook. 4th ed. New York: Wiley; 1999.

[43] Barrer RM, Barrie JA, Raman NK. Polymer 1962;3:605–14.

[44] Barrer RM, Barrie JA, Rogers MG. J Polym Sci, Part A 1963;1:2565–86.

[45] Van Amerongen GJ. Rubber Chem Technol 1964;37:1065–152.

[46] Paul DR, Kemp DR. J Polym Sci, Symp 1973;41:79–93.

[47] Kemp DR, Paul DR. J Polym Sci, Polym Phys 1974;12:485–500.